UCLA
UCLA Previously Published Works

Title
Altered cofactor regulation with disease-associated p97/VCP mutations

Permalink
https://escholarship.org/uc/item/9r4382bn

Journal
Proceedings of the National Academy of Sciences of the United States of America, 112(14)

ISSN
0027-8424

Authors
Zhang, Xiaoyi
Gui, Lin
Zhang, Xiaoyan
et al.

Publication Date
2015-04-07

DOI
10.1073/pnas.1418820112

Peer reviewed

Altered cofactor regulation with disease-associated p97/VCP mutations

Xiaoyi Zhang[a,b,1], Lin Gui[a,b,1], Xiaoyan Zhang[c], Stacie L. Bulfer[d], Valentina Sanghez[a], Daniel E. Wong[a], YouJin Lee[e], Lynn Lehmann[f], James Siho Lee[g], Pei-Yin Shih[g], Henry J. Lin[a], Michelina Iacovino[a], Conrad C. Weihl[e], Michelle R. Arkin[d], Yanzhuang Wang[c], and Tsui-Fen Chou[a,2]

[a]Division of Medical Genetics, Department of Pediatrics, Harbor–UCLA Medical Center, Los Angeles Biomedical Research Institute, Torrance, CA 90502; [b]College of Pharmaceutical Sciences, Capital Medical University, Beijing 100069, People's Republic of China; [c]Department of Molecular, Cellular and Developmental Biology, The University of Michigan, Ann Arbor, MI 48109-1048; [d]Small Molecule Discovery Center, Department of Pharmaceutical Chemistry, University of California, San Francisco, CA 94158; [e]Department of Neurology, Washington University School of Medicine, St. Louis, MO 63110; [f]NanoTemper Technologies, Inc., South San Francisco, CA 94080; [g]Division of Biology and Biological Engineering, California Institute of Technology, Pasadena, CA 91125

Dominant mutations in p97/VCP (valosin-containing protein) cause a rare multisystem degenerative disease with varied phenotypes that include inclusion body myopathy, Paget's disease of bone, frontotemporal dementia, and amyotrophic lateral sclerosis. p97 disease mutants have altered N-domain conformations, elevated ATPase activity, and altered cofactor association. We have now discovered a previously unidentified disease-relevant functional property of p97 by identifying how the cofactors p37 and p47 regulate p97 ATPase activity. We define p37 as, to our knowledge, the first known p97-activating cofactor, which enhances the catalytic efficiency (k_{cat}/K_m) of p97 by 11-fold. Whereas both p37 and p47 decrease the K_m of ATP in p97, p37 increases the k_{cat} of p97. In contrast, regulation by p47 is biphasic, with decreased k_{cat} at low levels but increased k_{cat} at higher levels. By deleting a region of p47 that lacks homology to p37 (amino acids 69–92), we changed p47 from an inhibitory cofactor to an activating cofactor, similar to p37. Our data suggest that cofactors regulate p97 ATPase activity by binding to the N domain. Induced conformation changes affect ADP/ATP binding at the D1 domain, which in turn controls ATPase cycling. Most importantly, we found that the D2 domain of disease mutants failed to be activated by p37 or p47. Our results show that cofactors play a critical role in controlling p97 ATPase activity, and suggest that lack of cofactor-regulated communication may contribute to p97-associated disease pathogenesis.

AAA ATPase | p97/VCP | MSP1 | p47 | steady-state kinetics

The p97 AAA [ATPase associated with diverse cellular activities; also called VCP (valosin-containing protein)] participates in key steps in ubiquitin-dependent protein quality control (1), autophagy (2, 3), membrane remodeling (4, 5), and numerous other fundamentally important cellular functions. p97 directs proteins to two major degradation systems: the proteasome and autophagy pathways. This key role of p97 underscores its importance in protein homeostasis and strongly implicates p97 in neurodegenerative diseases (6). Dominantly inherited missense mutations in p97 were initially associated with a rare degenerative disorder termed inclusion body myopathy with Paget's disease of bone and frontotemporal dementia (IBMPFD) (7, 8). Subsequently, it has been found that mutations in p97 cause a wider spectrum of degenerative diseases that includes amyotrophic lateral sclerosis (9–12) and parkinsonism (13). Thus, the acronym IBMPFD is insufficient. Moreover, mutations in the heterogeneous nuclear ribonucleoproteins hnRNPA2B1 and hnRNPA1 also cause a syndrome similar to conditions associated with VCP mutations (14). To account for the varied phenotypes and genetic etiologies of IBMPFD, it has been suggested that the term multisystem proteinopathy type 1 (MSP1) (14) be used to describe the phenotypic syndrome associated with mutations in p97. Disease mutants of p97 contribute to pathology by disrupting autophagosome

(2, 3) and endosome maturation, which leads to vacuolation, weakness, and muscle atrophy (15, 16). However, the molecular disease mechanisms associated with mutant p97 are still being investigated, with the eventual hope of developing therapeutic agents for these serious illnesses.

p97 assembles into a homohexamer, as revealed by X-ray crystallography (17, 18). A single monomer is composed of an N domain, which interacts with p97 cofactor proteins, and two ATPase domains, D1 and D2. The D1 and D2 domains form stacked hexameric rings, whereas the N domains extend outward, coplanar with the D1 ring. Most of the disease mutations occur in the N domain, whereas some occur in the D1 or the N–D1 linker region (see *SI Appendix*, Fig. S1A for examples). All p97 disease mutants tested thus far can form stable hexamers (19, 20) and exhibit increased D2 ATPase activity (19–23). Disease mutations lead to increased proteolytic susceptibility of the D2 ring (19). Structural and biochemical studies suggest that disease mutations alter N-domain and D1 conformations (20, 23,

Significance

Age-associated degenerative diseases have similar pathogenic mechanisms related to defects in protein homeostasis. p97/VCP (valosin-containing protein) is essential for coordinating protein degradation and is mutated in a multisystem degenerative disease that affects the central nervous system, muscle, and bone. p97/VCP is an enzyme in the AAA ATPases (ATPases associated with diverse cellular activities) family, which takes apart ATP and uses this energy to perform pivotal functions. We found that p97/VCP cofactors control its enzymatic activity. p97/VCP disease mutants behave abnormally due to lack of appropriate control by these cofactors. Correcting the function of the disease-associated proteins may be a desirable approach to developing safe treatment for fatal degenerative diseases. The next steps are to screen and characterize large panels of compounds to identify potential drugs that may correct the malfunction.

24) and cause defects in interdomain communication between neighboring subunits.

A major role of the N domain is to recruit cofactors (25, 26), such as the Npl4 (nuclear protein localization homolog 4) and Ufd1 (ubiquitin fusion degradation 1) heterodimers (27), and an array of 13 UBX (ubiquitin regulatory X) domain cofactors (28). By recruiting certain cofactor proteins, the N domain may link the mechanochemical activity of ATP hydrolysis to the unfolding or disassembly of substrate proteins. p47, the first p97 UBX cofactor discovered, is required for p97-mediated membrane fusion (29). Binding of p47 (also called NSFL1 cofactor p47 or UBX domain-containing protein 2C) to the N domain of p97 significantly reduces the diameter of the p97 ring (29) and inhibits wild-type p97 ATPase activity (30). Although actively studied, the physiological functions of p97–cofactor complexes and their mechanisms are largely unknown.

X-ray crystallography of p97 has revealed that the N domain of p97 is conformationally flexible (17, 18), adopting two primary conformations. In the up conformation, the N domain extends above the D1 ring, whereas in the down conformation, the N domain lies coplanar with the D1 ring. The conformation is nucleotide-dependent, that is, determined by the binding state of the D1 domain (17). It has been proposed that the flexibility of the N domain is crucial to ATP hydrolysis, because modifying the N domain reduces ATPase activity. Specifically, reducing N-domain mobility inhibits wild-type p97 ATPase activity (20). Moreover, removing the N domain (1~209) altogether was shown to block the enhanced ATPase activity of a disease mutant (20).

In wild-type p97, the N domains exist in a tightly regulated, heterogeneous arrangement of up and down conformations. In contrast, disease mutants exhibit dysregulated N-domain conformations (12, 17, 24). Crystal structures of two disease mutants showed all six N domains of the complex in the up conformation, a behavior that has been observed in only disease mutants (23). A recent study found that this uniform arrangement is a secondary effect of reduced ADP binding by the D1 domain, whose state controls N-domain conformation (23).

Altered conformation of the N domain in p97 disease mutants is further supported by atypical p97 cofactor binding in cells (31–33). Decreased binding to a UBX cofactor, UBXD1, is observed in 293T cells expressing p97 disease mutants and leads to a blockade of caveolin 1 trafficking (33). Intriguingly, disease mutants can coimmunoprecipitate more p47 and Npl4/Ufd1 heterodimers than WT p97, suggesting elevated binding affinities for p47 and Npl4/Ufd1 in mutant cells (31, 33). However, the consequences of altered binding to cofactors in cells that express mutant p97 have not been investigated biochemically. To provide a mechanistic understanding of cofactor-regulated ATPase activity, we analyzed the effect of p37 and p47 on the ATPase activity of WT and disease mutants of p97 in this study.

Results

p37- and p47-Regulated ATPase Activity of WT and Mutant p97. Pathogenic p97 mutations occur mostly in three regions of p97: the N domain, the N–D1 linker region, and the D1 domain (*SI Appendix*, Fig. S1A; arrows indicate representative mutants from these regions). These mutants are thought to affect the conformation and ATPase activity of p97. The models of WT and disease mutants in *SI Appendix*, Fig. S1B illustrate that (*i*) both D1 and D2 domains hydrolyze ATP, and (*ii*) N domains in a disease mutant have more up conformations, resulting in elevated basal D2 ATPase activity (20, 23). We first measured the ATPase activity of purified recombinant proteins and confirmed that all three mutants (R155H, L198W, and A232E) have higher basal ATPase activities than WT p97 (Fig. 1A).

To determine whether dysregulated N-domain conformations might affect p97 cofactor-regulated ATPase activity of disease mutants, we tested whether p47 affects ATPase activity of pathogenic p97 mutants and WT p97 in a similar manner. We measured the p97 ATPase activity of WT, R155H, L198W, and
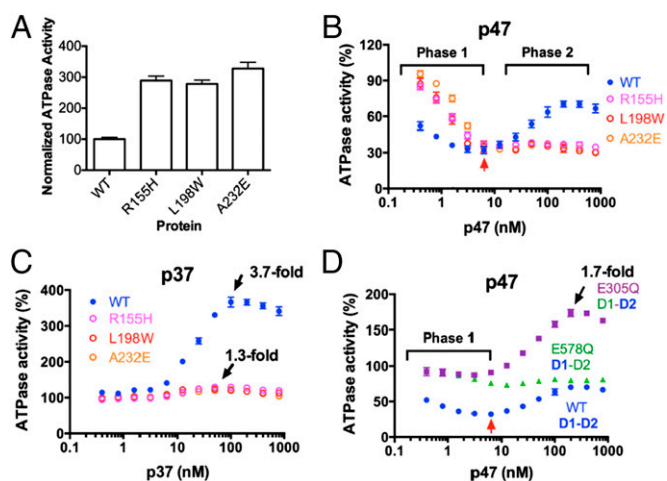

Fig. 1. Regulation of p97 ATPase activity by p37 and p47. (*A*) ATPase activity for p97 disease mutants normalized to WT activity and measured with 200 μM ATP (*n* = 6). For *B*–*D*, the activity of each p97 protein was normalized to its basal activity in the absence of cofactors. A red arrow marks the point at which the lowest activity was reached. (*B* and *C*) Normalized ATPase activities of WT, R155H, L198W, and A232E p97 in the presence of increasing amounts (0–800 nM) of p47 (*B*) or p37 (*C*), measured with 200 μM ATP. For *B*, *n* = 12, excluding L198W (*n* = 6). For *C*, *n* = 12. (*D*) The impact of p47 on ATPase activity was also measured for D1-E305Q and D2-E578Q p97 mutants (*n* = 12). Blue lettering indicates the active ATPase domain in each protein, and green lettering indicates the Walker B mutant. All error bars indicate ± SD.

A232E (at 4.17 nM hexamer) with increasing amounts of p47 (at 0–800 nM monomer) in the presence of 200 μM ATP (Fig. 1B). For each p97 protein, the % ATPase activity was normalized to the activity of p97 alone (without p47). We observed a biphasic inhibition of WT p97 by p47 (Fig. 1B, phases 1 and 2). At relatively lower concentrations of p47, p97 ATPase activity was strongly inhibited (Fig. 1B, phase 1; maximal 68% inhibition at 6.25 nM p47, indicated by a red arrow), consistent with a previous report (30). However, when p47 was added at higher stoichiometries than in the previous report (30), the inhibition was reduced to 30% (Fig. 1B, phase 2). Similar results were obtained when we carried out p47 titrations with 800 μM ATP for p47-regulated ATPase activity of WT p97 (*SI Appendix*, Fig. S1C) and with five times more WT p97 (20.8 nM hexamer, which was associated with a slight upshift of the curve; Fig. 1D).

For the R155H, L198W, and A232E disease mutants, which represent three regions of p97 (the N domain, N–D1 linker, and D1 domain, respectively), we detected a single inhibition phase. Moreover, their ATPase activity remained 68% inhibited with up to 800 nM p47 [with 200 μM (Fig. 1B, phase 1) or 800 μM ATP (*SI Appendix*, Fig. S1E)]. These results revealed two major differences between WT and p97 disease mutants: (*i*) p47 inhibited WT p97 threefold faster than the mutants at the initial phase, and (*ii*) the disease mutants lacked phase 2 (the rebound phase) when exposed to p47.

To determine whether this observation applied to other p97 cofactors, we performed similar experiments with the p97 cofactor known as p37 (also called UBX domain-containing protein 2B). The protein sequences of p37 and p47 are highly similar, but p37 is involved in distinct pathways required for Golgi and endoplasmic reticulum (ER) biogenesis (34–36). Interestingly, p37 activated WT p97 ATPase activity by 3.7-fold at 100 nM p37. In contrast, p37 activated p97 disease mutants by only 1.3-fold (see arrows in Fig. 1C). This pattern was not significantly affected when the ATP concentration was increased from 200 to 800 μM, for both WT p97 (*SI Appendix*, Fig. S1F) and its mutants (*SI Appendix*, Fig. S1G). These results define p37 as an activating cofactor of p97 ATPase—distinguishing it from p47, which is predominantly an

inhibitor. Moreover, there are substantial differences in the p37 control of WT versus mutant p97 ATPase activity.

To examine whether higher concentrations of p47 cause disease mutants to become less stable (as hexamers) than WT p97 and thereby lack the phase 2 rebound effect, we mixed 1.67 µM p97 hexamers with 80 µM p47 and fractionated the proteins by gel filtration. The ratio of p47 to p97 in the gel-filtration experiment corresponds to 200 nM p47 in the titration experiments (Fig. 1B). Previously, WT p97 has been shown to form a stable complex with p47 using a gel-filtration column (29). As shown in *SI Appendix*, Fig. S2A, both WT and R155H were eluted predominantly at fractions 18–20, corresponding to p97 hexamers. A similar amount of p47 was cofractionated with both p97 proteins. The excess amount of p47 formed stable trimers eluted at fractions 27 and 28 (*SI Appendix*, Fig. S2B), as seen in previous reports (29, 37). We concluded that lack of the phase 2 effect with p97 disease mutants is not due to denaturation of p97 by excess amounts of p47.

To estimate the amount of p37 or p47 trimer in the titration experiment, we quantitatively determined the equilibrium binding constant (K_D) for trimer formation for both p37 and p47 using microscale thermophoresis. The K_D values were 18.2 nM (±3.4 nM) and 6.9 nM (±1.9 nM) for p37 and p47, respectively (*SI Appendix*, Fig. S2 C and D). This indicates that at 6.9 nM p47, 3.45 nM p47 is in the form of trimers. Interestingly, the transition point from phase 1 to phase 2 occurred at 6.25 nM p47 (Fig. 1B, indicated by a red arrow), which is close to the K_D of p47 trimer formation. This result also suggests that the phase 2 rebound reaches maximal activity when the majority of p47 is in the form of trimers.

Contribution of D1 and D2 to p37- and p47-Regulated p97 ATPase Activity. To determine how the D1 and D2 ATPase domains of WT p97 contribute to p37 and p47 regulation of p97 ATPase activities, we compared the ATPase activities of WT p97 and Walker B mutants (D1-E305Q and D2-E578Q, which allow ATP and ADP binding but block activation of hydrolysis) (22, 38). We showed that p47 mediates an initial inhibitory phase (phase 1; *SI Appendix*, Fig. S1D) that requires catalytically active D1 and D2 ATP hydrolase domains, because both D1-E305Q and D2-E578Q lacked pronounced inhibition in phase 1 (which was observed for WT p97) (Fig. 1D). Activation of D1-E305Q was observed at 25 nM p47 and saturated at 200 nM p47. Thus, the rebound phase of WT p97 (Fig. 1B, phase 2) is mainly due to activation of D2 ATPase activity. Slight inhibition (26%) of D2-E578Q at 6.25 nM p47 (indicated by a red arrow in Fig. 1D) suggests that the initial inhibition (phase 1, maximal inhibition 68%) was caused by inhibiting both D1 and D2 in WT p97, when both D1 and D2 are capable of hydrolyzing ATP.

Because D2 is necessary and sufficient for the rebound phase of WT p97, and because disease mutants do not exhibit a rebound phase, we next evaluated how p47 regulates the D2 activity of the R155H or A232E disease mutants. The p47 titration curve for the R155H, D1-E305Q double mutant is relatively flat, with slight inhibition. It also lacks the activation phase observed for D1-E305Q (*SI Appendix*, Fig. S1H). The same result was obtained for A232E, D1-E305Q (*SI Appendix*, Fig. S1I). The titration curve for the p37 cofactor of WT p97 overlaps with the curve for D1-E305Q p97, whereas the curve for D2-E578Q p97 is flat (*SI Appendix*, Fig. S1J). Taken together, our data indicate that p37 activates D2 ATPase activity of WT p97, whereas p47 has dual effects on D1 and D2 activity in a concentration-dependent manner. Specifically, p47 inhibits both D1 and D2 at lower concentrations, whereas p47 slightly inhibits D1 but activates D2 at higher concentrations. Most importantly, the p37-mediated activation and the p47-mediated phase 2 rebound are not seen with the R155H, L198W, and A232E disease mutants. These results highlight the defect in cofactor-mediated ATPase activation in p97 disease mutants, and clearly show a defective function of p97 disease mutants.

Identification of the Region of p47 That Is Responsible for Phase 1 Inhibition of WT p97.

We found that p37 activates p97, without the phase 1 inhibitory effect observed for p47. To determine the origin of this major difference, we first searched for published structures of p47. Although p47 was discovered in 1997 (29), no X-ray or NMR structures for full-length p47 have been published. Electron microscopy has demonstrated that distinct conformational changes occur in p97 following binding to full-length p47 or partial versions of p47 (26, 29, 39). Specifically, binding to p47 reduces the diameter of the central channel within the p97 hexameric ring and changes the shape of the p97 ring from a hexagon to a pinwheel (29). Detailed NMR or X-ray structures are available for different truncated p47 domains, such as the N-terminal UBA (ubiquitin-associated) domain (37), the middle SEP (Shp eyes-closed p47) domain (37, 40), and the C-terminal UBX domain (25, 41). The obvious difference between p37 and p47 is that p37 lacks the UBA domain. Also, the p97–p37 pathway does not require ubiquitin for its function in maintaining Golgi structure during interphase and in reassembling the organelle during the later stages of mitosis (34). We therefore deleted the UBA domain (amino acids 1–46) from p47 to construct ΔUBA p47 and measured WT p97 ATP activity in the presence of increasing amounts of ΔUBA p47. The titration curves of WT p47 and ΔUBA p47 overlapped (*SI Appendix*, Fig. S1K), and suggested that the UBA domain of p47 does not contribute to the phase 1 inhibitory effect mediated by p47.

Because detailed structures are unavailable for either full-length p37 or p47, we continued our search for the phase 1 inhibitory region of p47 by aligning the amino acid sequences of p37 and p47. We found that amino acids 69–92 in p47 are completely absent from p37 (*SI Appendix*, Fig. S3A). To test the role of this region, we deleted amino acids 69–92 (Δ69–92 p47) and measured the effects on p97 activity (Fig. 2A, filled red squares). The Δ69–92 p47 deletion mutant completely abolished phase 1 and showed enhanced activation in phase 2, compared with WT p47 (Fig. 2A, filled blue circles). In fact, the WT ATPase activity titration curves of Δ69–92 p47 resemble the curve for WT p37 (Fig. 2A, filled red circles), with a single activation phase.

To potentially define the critical residues within amino acids 69–92 of p47, we found six acidic amino acids (one Asp and five Glu residues) within the region. To evaluate a role for these acidic residues in phase 1 inhibition, we deleted these acidic residues (to construct Δ83–90 p47) and also substituted the acidic amino acids with neutral residues [Asp to Asn and Glu to Gln, to make a variant designated 83–88 (DE$_5$ to NQ$_5$) p47]. All proteins [WT p37, WT p47, Δ69–92 p47, Δ83–90 p47, and 83–88 (DE$_5$ to NQ$_5$) p47] formed stable trimers during purification with a gel-filtration column (Superdex 75 10/300 GL; GE Healthcare). The purified trimer proteins were reanalyzed to confirm the formation of stable trimers (*SI Appendix*, Table S2). As shown in Fig. 2A, Δ83–90 p47 exhibited a slightly higher inhibitory phase 1 and a modestly higher phase 2 rebound (filled purple triangles); on the other hand, the curve of 83–88 (DE$_5$ to NQ$_5$) p47 overlapped with that of WT p47 (open orange diamonds). These results ruled out the possibility that electrostatic interactions generated by the negatively charged residues are a direct cause of the p97 ATPase inhibition, judging by the function of the three p47 variants. Instead, other interactions and/or the conformational differences related to the 69–92 region are needed for p47 to inhibit p97.

To reaffirm that WT p97 D2-ATPase activity is responsible for the phase 2 rebound effect with WT p47 (Fig. 1B), we demonstrated that Δ69–92 p47 activated D2-ATPase activity in p97 with a Walker B mutation in D1 (D1-E305Q; Fig. 2B, filled purple squares). In contrast, Δ69–92 p47 did not activate D1-ATPase activity in p97 with a Walker B mutation in D2 (D2-E578Q; Fig. 2B, filled green triangles). Taken together, we established that N-terminal amino acids 69–92 of p47 are responsible for the phase 1 inhibitory effect of WT p47. Removal of this region diminished the initial inhibitory effect and caused activation of D2-ATPase activity.
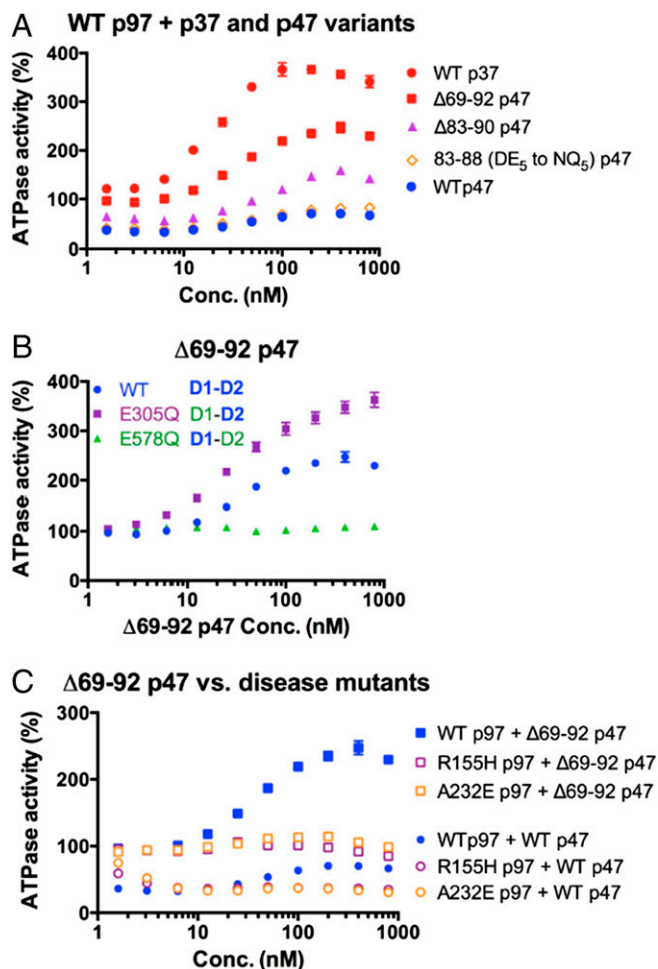
Fig. 2. Identification of amino acids 69–92 in p47 as an inhibitory region. (*A*) ATPase activities of WT p97 in the presence of p37, p47, and p47 variants (0–800 nM). $n = 6$, excluding p47 and Δ69–92 p47 ($n = 12$). (*B*) ATPase activities of WT and Walker B mutants (D1-E305Q and D2-E578Q) in the presence of Δ69–92 p47 (0–800 nM). $n = 12$, excluding E578Q ($n = 6$). (*C*) ATPase activities of WT and disease mutants of p97 in the presence of p47 versus Δ69–92 p47 (0–800 nM). $n = 12$, excluding R155H p97 + Δ69–92 p47 ($n = 6$). All error bars indicate ± SD.

Δ69–92 p47 Can Bind to p97 Disease Mutants but Cannot Activate Their ATPase Activity. Analysis of WT p97 in the presence of p47 variants in comparison with WT p37 revealed that p47 amino acids 69–92 play a critical role in inhibiting WT p97 ATPase activity (Fig. 2 *A* and *B*). As described above, WT p97 exhibits a rebound in ATPase activity when exposed to WT p47 at high concentrations (phase 2; Fig. 1*B*). Because p97 disease mutants have lost the phase 2 rebound normally associated with WT p47, we evaluated whether phase 2 activation might occur for disease mutants exposed to the activating variant (Δ69–92 p47). As shown in Fig. 2*C*, even Δ69–92 p47 failed to activate disease mutants, a result similar to p37 (Fig. 1*C*). Disease mutants of p97 remained consistently inhibited in the presence of WT p47, whereas WT p97 was able to recover at high concentrations of p47 (Fig. 2*C*). To determine whether the lack of activation of p97 disease mutants by p37 or Δ69–92 p47 was due to an inability to bind to p97, we used MagneHis Ni-Particles (Promega) to pull down His-tagged WT or p97 disease mutations in the presence of p37, p47, or p47 variants. Consistent with previous findings (42), we observed a strong reduction in the amount of F253S pulled down, and used this mutant as a control for no binding (*SI Appendix*, Fig. S3 *A* and *B*, lanes 3 and 8). We found that the binding of p47, Δ69–92 p47, and p37 to WT p97

(*SI Appendix*, Fig. S3 *B* and *C*, lanes 1–5) was almost identical to the binding of the disease mutants (lanes 6–10), indicating that lack of activation in the disease mutants was not due to differential binding.

We then used surface plasmon resonance (SPR) to quantitatively determine binding affinities. WT p47 and deletion p47 mutations bound similarly to WT p97 and disease mutants with two K_D values (~20 nM and ~1 µM) (*SI Appendix*, Fig. S4 and Table S3). Previous studies using isothermal titration calorimetry (ITC) determined K_D values of 500 nM (43) and 700 nM (44) for p47–p97 binding, whereas an SPR analysis with immobilized p47 detected a K_D of 31.3 nM (45). Our tight K_D is very close to the reported SPR value of 31.3 nM (45), and our weaker K_D is closer to the ITC data. The two different K_D values we obtained could be attributed to one or more of the following: (*i*) p47 has two distinct binding sites for p97 (26, 37); (*ii*) the binding of p47 monomers vs. p47 trimers (37); or (*iii*) p97 adopts different conformations that bind cofactors differently. In contrast, the binding of p37 was best fit to a 1:1 binding model with a K_D of ~20 nM (similar to the tight binding K_D for p47). However, a limitation of this experiment was that at higher p37 concentrations (>256 nM), we started to observe significant nonspecific binding (*SI Appendix*, Fig. S4*A*), which prevented the measurement of a potential second binding affinity. Together, our results indicated that Δ69–92 p47 and WT p47 can bind to WT p97 and disease mutants similarly. Interestingly, although residues 69–92 in p47 were not important for the direct binding to p97, they do influence the communication from the N-domain binding sites to the D1 or D2 domains to activate D2 ATPase activity.

Steady-State Kinetic Analysis of p97–p47 Complexes. We measured steady-state kinetic constants (k_{cat}, K_m, and k_{cat}/K_m) to understand the effects of p47 on regulating WT p97 and its disease mutants. In comparison with WT p97, the disease mutants R155H, L198W, and A232E had 2.8- to 3.3-fold higher values of k_{cat} (the maximum rate of ATP turnover) and 2.9- to 3.6-fold lower values of K_m (the Michaelis Menten constant, the ATP concentration necessary for half-maximal ATPase activity) (Fig. 3*A*). Thus, the resulting 9- to 12-fold increase in the apparent second-order rate constant (k_{cat}/K_m), also known as the catalytic efficiency, indicates an order-of-magnitude increase in the ATPase rate associated with disease-causing point mutations.

We then evaluated p47 concentration effects on WT and three disease mutants of p97 under steady-state kinetic conditions and generated Michaelis Menten curves (Fig. 3 *B* and *C*). For WT p97, 12.5 nM p47 lowered both the k_{cat} and K_m, by 2.6- and 3.6-fold, respectively. At 800 nM, p47 lowered the K_m by 3.8-fold but had no effect on the k_{cat} (Fig. 3*B*). For the A232E p97 mutant, the Michaelis Menten curve at 12.5 nM p47 was identical to the curve at 800 nM p47 (Fig. 3*C*). This striking difference prompted us to evaluate p47 concentration effects more closely for WT p97 and disease mutants with single mutations in the N domain (R155H), N–D1 linker region (L198W), and D1 domain (A232E) (Fig. 3 *D–F*). At low p47 concentrations, the k_{cat} and K_m of WT p97 decreased, and as a result the k_{cat}/K_m values were constant up to 12.5 nM p47 (one p47 trimer to one p97 hexamer). When p47 concentrations were increased further, the k_{cat} rebounded back to the basal p97 value and the K_m remained low, resulting in a maximum catalytic efficiency (k_{cat}/K_m, 4.4-fold higher, indicated by an arrow in Fig. 3*F*). The concentration-dependent effects of p47 on all three disease mutants were similar for both k_{cat} (Fig. 3*D*) and K_m (Fig. 3*E*). The k_{cat} values reached a minimum at 12.5 nM p47, with activities 3.6- to 3.8-fold lower than the basal level (0 nM p47; red box). The k_{cat} values remained constant through 800 nM p47. The K_m values also decreased up to 2.8-fold, resulting in k_{cat}/K_m values less than 2-fold lower than basal levels (with no p47) (Fig. 3*F*). Taken together, p47 regulated the steady-state kinetic behavior of WT and disease mutants in a distinct manner. ATP binding affinities were increased for WT p97 more than for the disease mutants, with increasing amounts of p47. On the other hand, the ATP hydrolysis rates for the disease mutants were significantly reduced by p47 more so than for WT p97. The overall
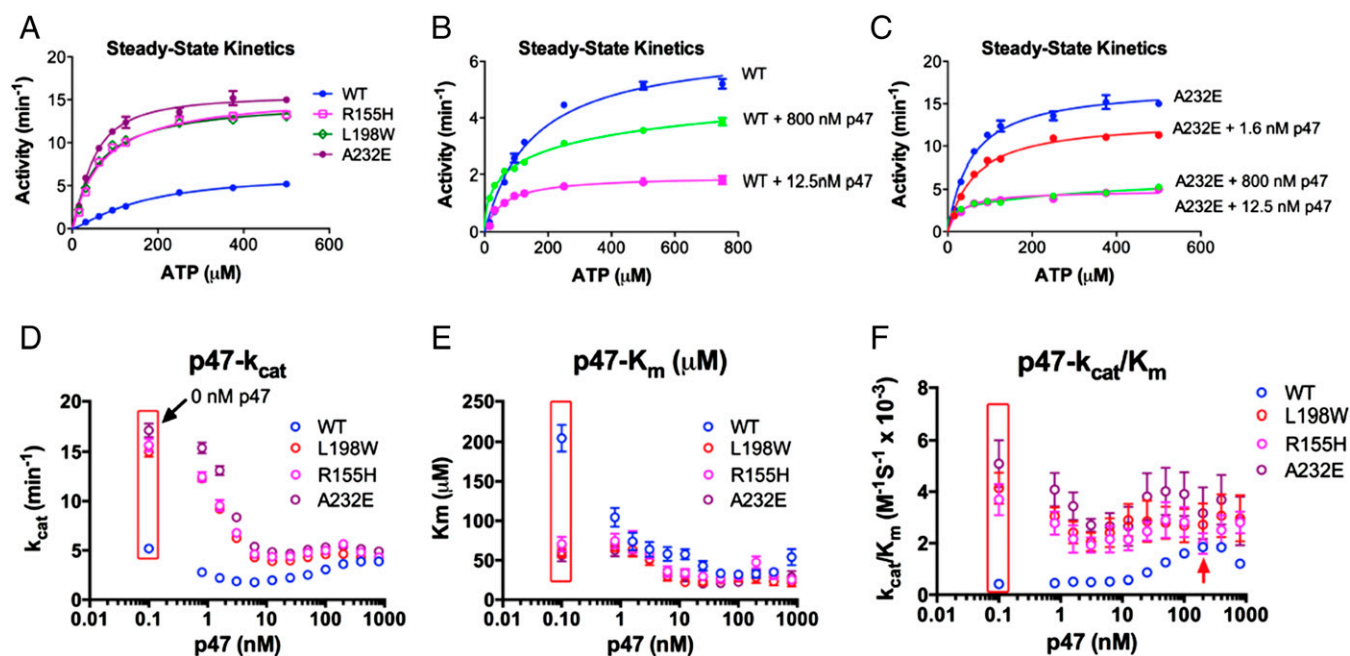
Fig. 3. Steady-state kinetic analyses of p47–p97 complexes. (*A*) Michaelis Menten curves for ATP hydrolysis by WT, R155H, L198W, and A232E mutants of p97. (*B*) Michaelis Menten curves for WT, WT with 12.5 nM p47, and WT with 800 nM p47. (*C*) Michaelis Menten curves for A232E, A232E with 1.6 nM p47, A232E with 12.5 nM p47, and A232E with 800 nM p47. (*D*) p47 concentration effects on the turnover number (k_{cat}, min^{-1}) of WT, R155H, L198W, and A232E. (*E*) p47 concentration effects on the Michaelis Menten constant (K_m, μM) of WT, R155H, L198W, and A232E. (*F*) p47 concentration effects on the catalytic efficiency (k_{cat}/K_m, M$^{-1} \cdot$s$^{-1} \times 10^{-3}$) of WT, R155H, L198W, and A232E. Experiments were performed using p97 proteins at 4.17 nM hexamer. The 0 nM p47 titration points are boxed in red. All error bars indicate ± SEM ($n = 5$).

p47 effect on the catalytic efficiency (k_{cat}/K_m) was positive for WT but negative for disease mutants at higher amounts of p47.

Steady-State Kinetic Analysis of Walker B Mutant p97–p47 Complexes. To gain a better understanding of how D1 and D2 ATPase activities of WT and disease mutants are regulated by p47, we performed steady-state kinetic experiments with Walker B mutants (which can bind to ATP but cannot hydrolyze it) at D1 (D1-E305Q) or at D2 (D2-E578Q) for both WT p97 and disease mutants. We found that at low p47 concentrations, p47 cannot lower the k_{cat} of the D2 ATPase, when D1 cannot hydrolyze ATP (see E305Q, Fig. 4*A*, data in green circles compared with data in blue circles for WT p97). At 800 nM p47, the k_{cat} of D1-E305Q becomes substantially greater than that of WT p97. The resulting k_{cat}/K_m curves are similar for WT and D1-E305Q. All of the curves for D2-E578Q are flat, indicating that p47 does not affect the kinetic behavior of D1 significantly, when D2 cannot hydrolyze ATP (Fig. 4 *A*–*C*, red circles). The different effects of p47 on WT, D1-E305Q, and D2-E578Q again confirmed that cofactor-mediated communication between the N domain, D1, and D2 is a dynamic process that controls the ATP hydrolysis cycle.

Binding of p47 slightly inhibited D1 catalytic efficiency but stimulated D2 catalytic efficiency. Cross-inhibition of the maximal activity of D2 by D1 is much more striking in the presence of p47. Even at 0.8 nM p47, the k_{cat} of D2 alone (D1-E305Q) is 2.4-fold higher than that of WT p97 (in which both D1 and D2 can hydrolyze ATP). At 800 nM p47, the k_{cat} of D2 is 4-fold greater than that of WT (Fig. 4*A*). These observations are consistent with negative cooperativity between the D1 and D2 rings, which was shown for mouse p97 (46). In addition, recent studies show that D1 ATP hydrolysis inhibits D2 ATPase activity, and vice versa (22, 23). We then made double mutants (A232E, D1-E305Q and A232E, D2-E578Q) to assess the impairment of the p47-mediated ATPase cycle in a disease mutant of p97. Steady-state kinetic analysis revealed that D1-E305Q had no effect on basal k_{cat} and K_m values for A232E (Fig. 4 *D* and *E*, red boxes). Thus, the elevated ATPase activity in disease mutants comes

from the k_{cat} of D2 (2.7-fold higher for A232E, D1-E305Q compared with D1-E305Q). A232E, D2-E578Q was kinetically identical to D2-E578Q (Fig. 4 *A* and *D*), as found in previous reports (20, 22, 23). Interestingly, p47 had no effect on the k_{cat} of D2 in the A232E mutant, when D1 lost the ability to hydrolyze ATP (Fig. 4*D*, A232E, D1-E305Q, orange circles). This finding contrasts with the drastic decrease in the k_{cat} of A232E p97 (Fig. 4*D*, purple circles) with increasing amounts of p47. Another major difference between WT and A232E is that p47 produced a greater increase in the K_m of A232E, D1-E305Q compared with D1-E305Q, meaning that p47 decreased the overall catalytic efficiency (k_{cat}/K_m) of A232E, D1-E305Q up to 5-fold (Fig. 4*F*). Thus, the p47-regulated ATPase cycle is clearly affected by disease mutations (Fig. 4). Moreover, the ATP hydrolysis states of D1 significantly impact how D2 responds to p47. For example, with WT p97, ATP hydrolysis by D1 blocked activation of D2 by p47 (as shown by k_{cat} values; Fig. 4*A*). However, with the disease mutant, ATP hydrolysis by D1 was required for the enhanced ATP binding to D2 mediated by p47 (as shown by K_m values) (Fig. 4*E*). These results strengthen the significance of the dynamic communication among the N, D1, and D2 domains during the ATPase cycle. The apparent steady-state kinetic behavior of D1 is unaffected by p47. Specifically, neither the overall k_{cat} nor K_m from the six ATP binding sites of D1 appeared to respond to p47. The presence of D1 ATP hydrolysis had dramatic effects on how D2 responded to p47, by reducing the ATP hydrolysis rate (k_{cat}) and by maintaining tighter ATP binding (K_m).

Steady-State Kinetic Analysis of p97–p37 Complexes. To evaluate p37 activation of WT p97 ATPase activity in detail, we performed steady-state kinetic analysis for WT and A232E in the presence of 800 nM p37 (Fig. 5*A*). We observed an 11-fold increase in the catalytic efficiency (k_{cat}/K_m) of WT p97, the result of a 2.2-fold k_{cat} increase and a 5-fold K_m decrease. In contrast, the k_{cat}/K_m value of A232E increased only 1.8-fold (Fig. 5*A*). Given the substantial difference in p37-regulated ATPase activity between WT and A232E, we then investigated concentration-dependent effects
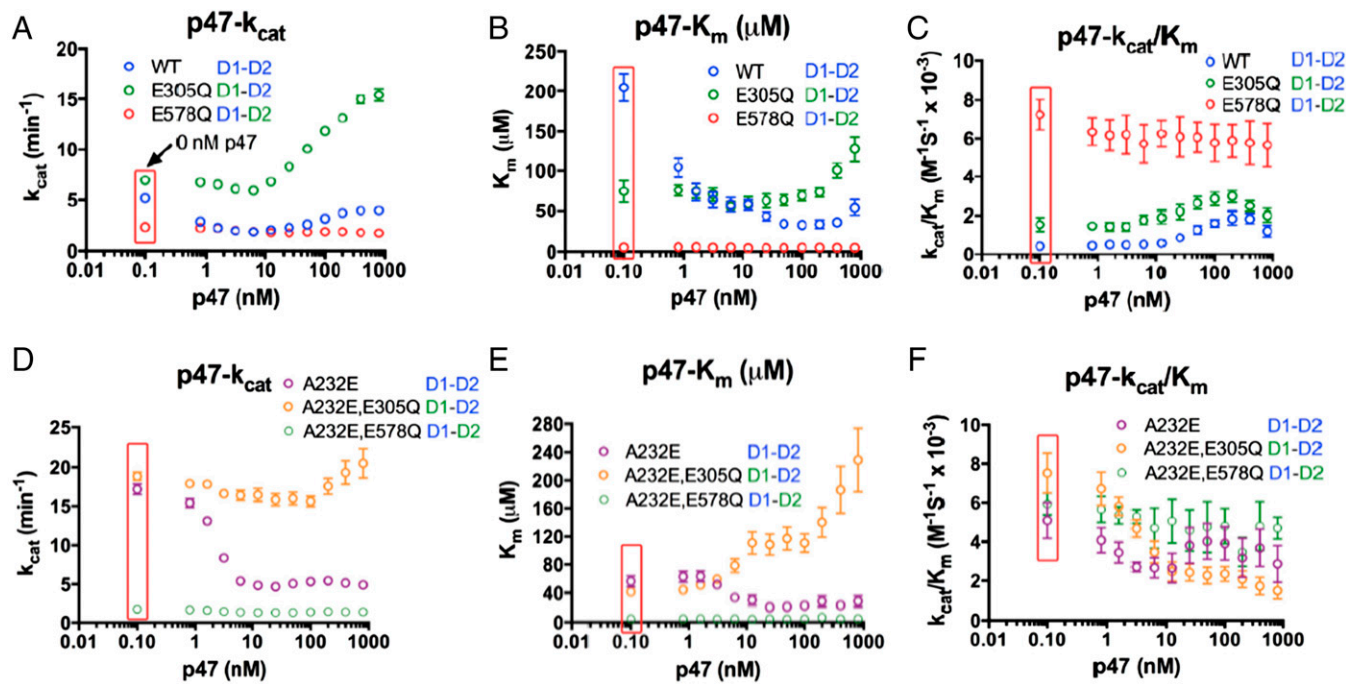
Fig. 4. Concentration-dependent effects of p47 on steady-state kinetic behavior. For WT, D1-E305Q, and D2-E578Q p97 proteins, values of (A) k_{cat}, (B) K_m, and (C) k_{cat}/K_m are shown. For A232E and double mutants A232E, D1-E305Q and A232E, D2-E578Q, values are shown for (D) k_{cat}, (E) K_m, and (F) k_{cat}/K_m. Experiments were performed using p97 proteins at 4.17 nM hexamer. p47 titrations were performed from 0 nM (boxed in red) to 800 nM. All error bars indicate ± SEM ($n = 5$).

of p37 for WT p97, D1-E305Q, A232E, and the double mutant A232E, D1-E305Q (Fig. 5 B and C). For p37 concentrations <6.25 nM, no significant change was detected in k_{cat} values (Fig. 5B). The k_{cat} values of D1-E305Q started to increase at 6.25 nM and reached a maximum at 100 nM p37 (increasing from 6.3 to 23.3 min^{-1}). WT p97 k_{cat} values increased from 6.7 to 15.1 min^{-1}. A232E k_{cat} values increased from 19.2 to 25.6 min^{-1}, and those for A232E, D1-E305Q increased from 17.2 to 29.7 min^{-1}. The p37-mediated increase in turnover number (k_{cat}) of D2 ATPase activity is higher when D1 cannot hydrolyze ATP for both WT and A232E. These results confirm the cross-inhibition between D1 and D2 ATPases, as observed previously for p47-regulated ATPase activity (Fig. 4A) and basal p97 ATPase activity (22, 23).

Regarding the effects of p37 on K_m values, p37 decreased the K_m of WT p97 from 180 to 32 μM, but no significant change was observed for mutant p97 proteins (Fig. 5C). Last, p37 enhanced the catalytic efficiency (k_{cat}/K_m) of WT p97 from 0.6×10^3 M^{-1}·s^{-1} to 6.5×10^3 M^{-1}·s^{-1} (11-fold), and increased the catalytic efficiency of D1-E305Q from 1.0×10^3 M^{-1}·s^{-1} to 6.0×10^3 M^{-1}·s^{-1} (6-fold). Furthermore, the k_{cat}/K_m curve of D1-E305Q was shifted to the left (Fig. 5D, red arrow). The shift indicates that p37 is a 4-fold more potent activator for D1-E305Q than for WT p97 (Fig. 5D). Consistent with our titration result (Fig. 1C), the maximal increase in the k_{cat}/K_m value of A232E p97 is 1.8-fold, and the k_{cat}/K_m value of the double mutant (A232E, D1-E305Q) decreased slightly, from 6.8×10^3 to 5.1×10^3 M^{-1}·s^{-1}.

Taken together, the steady-state kinetic analyses revealed that p37 is a strong activator for WT p97 ATPase activity. The p37 cofactor not only enhanced the rate of ATP hydrolysis (k_{cat}) but also improved the apparent ATP binding affinity to WT p97 (K_m). Interestingly, when D1 was locked in the ADP/ATP-bound state by a Walker B mutation, p37 was an even more potent activator for the D2 ATPase, mainly through enhancing the ATP hydrolysis rate. The activator effect was absent for the p97 disease mutant.

p97-Mediated Postmitotic Golgi Reassembly Assays. To demonstrate functional importance beyond ATPase activities, we showed that

a disease mutant is hyperactive and less responsive to activation by p37 in postmitotic Golgi membrane fusion in a well-characterized in vitro reconstitution assay (36, 47). Specifically, the R155H disease mutant is 2.5 times more active than WT in this p97-mediated postmitotic Golgi reassembly assay (*SI Appendix,* Fig. S5A, compare column 2 with 3). For WT p97, addition of the p37 trimer at a 1:1 ratio increases the reassembly activity by 6.9-fold (*SI Appendix,* Fig. S5A, compare column 2 with 4). At a 1:8 ratio of WT p97 to p37, the reassembly activity increases 11-fold (*SI Appendix,* Fig. S5A, compare column 2 with 5). However, for R155H p97, addition of the p37 trimer at ratios of 1:1 and 1:8 increases reassembly only 3.9-fold (*SI Appendix,* Fig. S5A, compare column 3 with 6 or 7). We then compared the effects of p37, p47, and Δ69–92 p47 in the Golgi reassembly assay (*SI Appendix,* Fig. S5B). For p47, there is no difference in reassembly between 1:1 and 1:8 ratios of p97 hexamer to p47 trimer complexes (*SI Appendix,* Fig. S5B, compare column 3 with 4). Both ratios increased the reassembly activity 7.7-fold (*SI Appendix,* Fig. S5B, columns 2–4). When Δ69–92 p47 was added at a ratio of 1:1, we saw the reassembly activity increase by 7.2-fold (*SI Appendix,* Fig. S5B, compare column 2 with 5). At a 1:8 ratio of WT p97 to Δ69–92 p47, the increase was 12.2-fold (*SI Appendix,* Fig. S5B, compare column 2 with 6). The activating cofactor, p37, generated a 12.2-fold increase in the reassembly activity at a 1:1 ratio (*SI Appendix,* Fig. S5B, compare column 2 with 7) and a 13.8-fold increase at a 1:8 ratio (*SI Appendix,* Fig. S5B, compare column 2 with 8). Taken together, results from this in vitro reconstituted, functional p97 assay are consistent with results on ATPase activity.

p47 Improves p97/VCP Disease-Associated Autophagy Impairment. The ATPase activity and in vitro reconstituted Golgi reassembly results demonstrated a concentration-dependent effect of the p47 cofactor for WT and disease mutants of p97 proteins. We reasoned that increased expression of p47 may correct the defect in autophagy seen in p97 disease mutant-expressing cells. It has been previously established that the yeast homolog of p47, Shp1, is essential for autophagosome biogenesis (48), although whether mammalian p47 behaves similarly has not been established. To
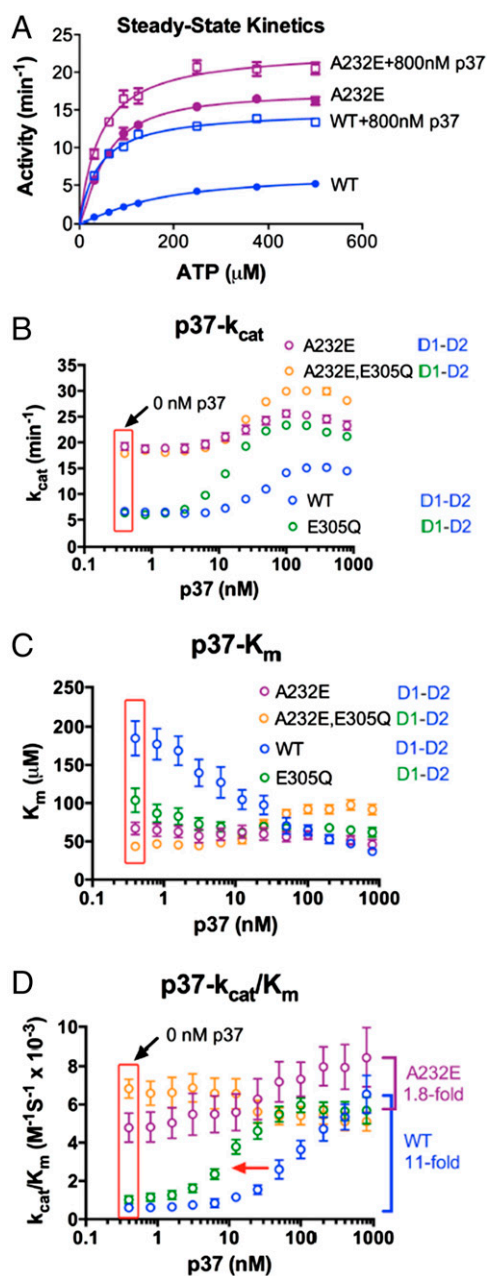
Fig. 5. Steady-state kinetic analyses of p37–p97 complexes. (*A*) Steady-state kinetic analyses of WT and A232E p97 ATP hydrolysis were performed with and without 800 nM p37. p97 proteins were used at 4.17 nM hexamer. (*B*–*D*) Dependence of k_{cat} (*B*), k_m (*C*), and k_{cat}/K_m (*D*) values on p37 concentration is shown for WT p97 and A232E, D1-E305Q, and a A232E, D1-E305Q double mutant (4.17 nM hexamer). p37 titrations were performed from 0 nM (boxed in red) to 800 nM. All error bars indicate ± SEM (*n* = 5).

assess this possibility, we expressed mammalian Flag-p47 in human osteosarcoma U2OS cells and performed an "autophagic flux" assay (2). In agreement with yeast Shp1, mammalian p47 increased the amount of LC3-II produced, consistent with an activation of autophagy (when comparing the increase in LC3-II protein in *SI Appendix*, Fig. S6A, lanes 3 and 4). We have previously established that p97 disease mutations impair autophagic flux, leading to an accumulation of LC3-II and p62 in U20S cells stably expressing mutant p97 (2). To see whether p47 could improve autophagy in these cells, we expressed Flag-p47 and immunoblotted for LC3 and p62. As previously reported (2), the

steady-state levels of LC3-II and p62 are increased in p97 mutant-expressing cells. Coexpression of p47 decreases the levels of LC3-II and p62, consistent with a correction in the autophagic block due to p97 mutations. As shown in *SI Appendix*, Fig. S6B, L198W and A232E lines have higher levels of p62 and the lipidated LC3-II (*SI Appendix*, Fig. S6B, compare lane 7 or 10 with 4). Expression of Flag-p47 results in a significant decrease in p62 and LC3-II (*SI Appendix*, Fig. S6B, compare lane 7 with 8 or 9 or lane 10 with 11 or 12). Taken together, these data indicated that overexpression of Flag-p47 can rescue the defect in p97 disease mutant overexpression in U2OS cells.

Implications for Future Therapeutic Development by Targeting Disease Mutants of p97. We previously identified three potent, ATP-competitive p97 inhibitors (DBeQ, ML240, and ML241; *SI Appendix*, Fig. S7A) (49, 50). In addition, Nerviano Medical Sciences and Genentech identified NMS-873 (*SI Appendix*, Fig. S7A) as a potent non–ATP-competitive p97 inhibitor (51, 52). To investigate whether these four p97 compounds inhibit the ATPase activity of the R155H p97–p47 complex, IC_{50} values were determined for p97 (with BSA as control) and for the p97–p47 complex (with both WT p97 and R155H; *SI Appendix*, Fig. S7 *B*–*E*). Compared with the WT p97–p47 complex, NMS-873 was three times more effective and ML240 was two times more effective against the R155H p97–p47 complex. Our data suggest that it is possible to develop a mutant–cofactor complex selective inhibitor or activator. Selective inhibition or activation of the mutant subunit may rescue mutant malfunction within cells. However, future work will be required to screen for more selective compounds for the disease mutant to further test this hypothesis.

Discussion

Regulation of WT p97 ATPase Activity. Regulation of ATPase or GTPase activity occurs extensively in nature, through various control mechanisms. For example, Ras superfamily GTPase activation occurs via a canonical nucleotide exchange mechanism, through binding to guanine nucleotide exchange factor proteins. These proteins facilitate release of GDP, allowing GTP to bind, thereby activating the enzyme (53). Another well-characterized model of regulation involves the 90-kDa heat shock protein (Hsp90), a dimeric molecular chaperone with weak basal ATPase activity. Binding to its cochaperone, Aha1 (activator of Hsp90 ATPase), at a ratio of one Aha1 per Hsp90 dimer stimulates the ATPase activity of Hsp90 by threefold (54). Human Hsp90 ATPase has a K_m value of 324 μM for ATP and a k_{cat}/K_m of 46 $min^{-1} \cdot M^{-1}$ (55), which is about ninefold less than that of human p97. With such a low basal ATPase rate, Hsp90 not only needs an activating cochaperone but also requires inhibiting cochaperones to reduce activity (56). Additional complexities in the control of the p97 AAA protein come from occurrence of intradomain communication within the same protomer and interdomain communication between neighboring protomers. For example, interprotomer motion transmission between the D1 and D2 ATPase domains of p97 has been shown to be critical for the ERAD (endoplasmic reticulum-associated degradation) function of p97 (57, 58). Biochemical studies indicate that p97 disease mutations cause defects in interdomain communication between neighboring subunits (23).

Several p97 cofactors (also called adaptors or interacting proteins) have been identified, although they have not been characterized as well as the regulators described above. It is believed that cofactors of p97 mediate ATPase function and likely determine substrate selection (59). However, investigators have not emphasized regulation of p97 ATPase activity by these proteins. In a recent study, we found that the p47 UBX cofactor and p97 disease mutations dramatically affect the potency of p97 ATPase inhibitors (22). To facilitate development of potent anti-p97 drugs, we aim to characterize cofactor-mediated regulation of this essential AAA enzyme in detail.

Our study provides mechanistic insight into cofactor-regulated p97 ATPase activity. We initially focused on p47, because it was

the only cofactor previously shown to affect p97 ATPase activity (30). Through extensive analysis, we demonstrated that regulation of p97 ATPase by p47 occurs biphasically. We do not have direct evidence on how this process occurs, but we propose several explanations. At low p47 concentrations (0.4–12.5 nM p47 monomer), p47 promotes an ADP-locked state and/or prevents ATP from binding to D1. This inhibits both D1 and D2 ATPases, because the binding of ATP to D1 is required for ATP hydrolysis by D2 to occur (22, 60, 61). Therefore, locking D1 in an ADP-bound state prevents ATP from binding and consequently inhibits the activity of both D1 and D2. This explanation is supported by activity of the Walker B mutant D1-E305Q, which shows lack of inhibition. Specifically, because the D1 domain in the D1-E305Q mutant can bind ATP, but cannot hydrolyze it, ATP remains bound, and ATP-bound D1 signals for D2 to increase its activity in the presence of p47 (Figs. 1*D* and 4*A*). In further support of this explanation, there is only slight inhibition of D1 activity when the mutation occurs in D2 (i.e., the D2-E578Q mutant) (Fig. 1*F*). At higher p47 concentrations (25–800 nM p47 monomer), p47 promotes an open state of D1, which facilitates more ATP binding to D1. Thus, D2 activity is stimulated, because more D2 sites are able to hydrolyze ATP (Figs. 1*D* and 4*A*).

We consider possible mechanisms for the transition from phase 1 (occurring at lower p47 concentrations) to phase 2 (occurring at higher p47 concentrations). Deletion analysis has shown that p47 has two p97 binding sites (26, 37). Binding affinities between p97 and p47 indicate two K_D values (26 and 1,400 nM) (*SI Appendix*, Fig. S4 and Table S3). Therefore, several explanations for the transition may be possible. For example, (*i*) self-association of UBA/UBX domains within the same p47 monomer may occur at lower p47 concentrations, as suggested for UBXD7 (62). Self-association may prevent p47 from activating D2. We ruled out this mechanism by making a ΔUBA variant (47–370 p47), which cannot self-associate. The titration result was identical to the curve for WT p47 (*SI Appendix*, Fig. S1*K*). Alternatively, (*ii*) there may be differences in p97 conformations for binding at one versus two sites, or (*iii*) p47 monomers may assemble into trimers (37). Such trimers may, in turn, affect how p47 regulates p97 ATPase. Finally, (*iv*) the 69–92 region of p47, which has a dominant inhibitory effect at lower p47 concentrations, may induce a conformational change that allows p97 reactivation in phase 2 in response to higher p47 concentrations. Fig. 6 shows a possible model to explain the transition caused by p47 monomers and trimers. This model and the model with two binding sites are not mutually exclusive, because both models could occur concurrently. For example, the affinities of two p97 binding sites may differ for p47 monomers and trimers. The tight binding site may be the main site for p47 monomers, whereas the weaker binding site may be preferred by p47 trimers— and this difference may trigger the transition.

Steady-state kinetic analysis revealed that the K_m of ATP for WT p97 falls significantly with increasing amounts of p47 (Fig. 3*E*), which provides an explanation for why p47 decreases the potency of p97 ATP-competitive inhibitors but not an allosteric inhibitor (22). In the presence of p47, ATP binding to WT p97 becomes stronger, and therefore p97 ATP-competitive inhibitors are unable to inhibit p97 as effectively (compared with p97 alone). We confirmed this result for WT p97–p47 complexes and also determined the potencies of p97 inhibitors against R155H p97–p47 complexes (*SI Appendix*, Fig. S7). NMS-873 (an allosteric inhibitor) and ML240 (an ATP-competitive inhibitor) were two- to threefold more potent against the R155H p97–p47 complex. This result demonstrated that the conformations of the WT p97–p47 complex and the R155H p97–p47 complex are likely to be different, thus affecting how inhibitors bind to p97. Our data suggest that a potential future direction may be to develop selective inhibitors or activators for mutant–cofactor complexes and to evaluate their ability to correct the malfunction of p97 disease mutants.

Our study uncovers p37 as the first p97-activating cofactor, to our knowledge, which enhances the catalytic efficiency (k_{cat}/K_m)
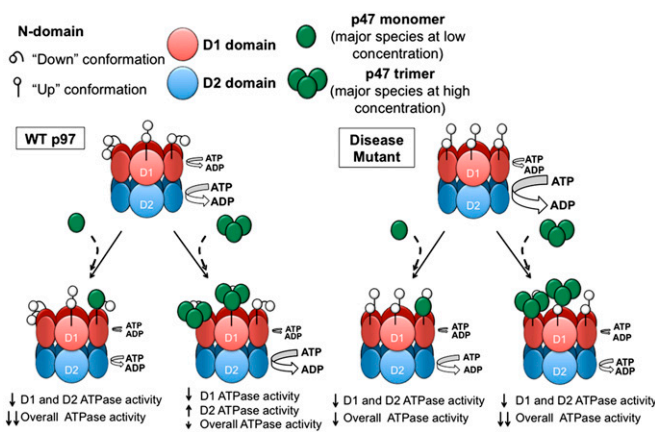

Fig. 6. Cofactor-induced changes in p97 ATPase activity. Diagram showing the domain representation of human p97 and the p47 cofactor. Illustrations depict changes in p97 ATPase activity of WT and disease mutants caused by the presence of p47.

of WT p97 by 11-fold. p37-mediated activation predominantly affects p97's D2 activity (*SI Appendix*, Fig. S1*J*). Steady-state kinetic analysis reveals that p37 is an even more potent D2 ATPase activator when D1 cannot hydrolyze ATP (Fig. 5*D*, comparing WT with D1-E305Q). Furthermore, p37 reduced the ATP K_m value for WT p97 (Fig. 5*C*), which suggests that p97 ATP-competitive inhibitors will have difficulty in inhibiting p97–p37 complexes as well.

Dysregulation of p97 ATPase Activity in Disease Mutants. Differences between WT and disease mutants of p97 reported previously suggest that abnormal interactions with p97 cofactors in cells and the hyperactive D2 ATPase activity for the mutants are the keys to the pathogenic mechanisms. However, the missing link between the regulation of ATPase activity and p97 cofactors prompted us to carry out a simple initial comparison. Specifically, we checked whether p97 disease mutants could be inhibited by p47. The results clearly show that the responses to p47 that occur in both phase 1 and phase 2 are significantly different from what is seen with WT p97 (Fig. 1*B* and *SI Appendix*, Fig. S1*B*).

p97 activity at 0.4–12.5 nM p47 monomer. The inhibitory effect of p47 on p97 disease mutants at lower p47 levels can possibly occur in the same way as inhibition of WT p97. At low p47 concentrations (0.4–12.5 nM p47 monomer), p47 promotes an ADP-locked state and/or prevents ATP from binding to D1, thereby inhibiting the ATPase activity of both D1 and D2. This explanation is supported by the Walker B double mutant, R155H, D1-E305Q, which lacks strong phase 1 inhibition. The Walker B mutation (E305Q) allows ATP binding to D1 but prevents ATP hydrolysis (meaning that D1 can bind to ATP but cannot hydrolyze it) (*SI Appendix*, Fig. S1*H*, green squares). Moreover, phase 2 inhibition is also missing for R155H, D1-E305Q at higher p47 concentrations (25–800 nM p47 monomer). At 0.4–12.5 nM p47 monomer, p47 strongly reduced the k_{cat} of disease mutants (Fig. 4*D*), suggesting that p47 can inhibit the ATPase rate through an N-domain binding event that affects D1 and D2 ATPase activities, even at saturating ATP concentrations.

p97 activity at 25–800 nM p47 monomer. At 800 nM p47, the k_{cat} values of disease mutants are similar to those of WT p97 (Fig. 4*D*). However, the k_{cat} values of WT p97 increase from 25 to 800 nM p47, whereas the k_{cat} values of disease mutants remain constant over 25–800 nM p47, eventually converging with the WT k_{cat} values at 800 nM p47. In fact, this is the general trend observed when comparing the K_m and the overall k_{cat}/K_m values. Thus, despite the physical and functional differences between WT p97 and disease mutants, excess amounts of p47 (64 p47 trimers per p97 hexamer) can cause disease mutants to adopt the same steady-state kinetic behavior as WT p97. We have shown

that overexpressing p47 can rescue the autophagy defect caused by overexpression of disease mutants in U2OS cells (*SI Appendix*, Fig. S6). More work needs to be done to investigate the potential of this finding, such as determining whether the disease phenotype can be rescued by modifying its behavior.

p97 activity at 0.4–800 nM p37 monomer. To our knowledge, p37 is the first p97-activating UBX cofactor we identified and has little effect on disease mutants (Figs. 1*C* and 5). One possible explanation is that the p97 mutants exist in a hyperactive conformation that is normally induced by binding to p37. Therefore, binding of p37 to a disease mutant cannot increase ATPase activity above its usual levels. It is also possible that the altered domains or abnormal interdomain communication caused by the disease mutation makes p97 unable to communicate the p37 binding effect from the N domain to the D1 and D2 domains of p97 (*SI Appendix*, Fig. S8*A*).

Turning p47 into a p37-Like p97 Activator by Deleting Amino Acids 69–92. Golgi membrane fusion mediated by p97 requires two distinct cofactors, p47 and p37 (29, 34). The p97–p47 pathway requires binding to monoubiquitin via the UBA domain of p47 (amino acids 1–45) (5, 36). The p97–p37 pathway does not require ubiquitin for its functions (34). p37 lacks the UBA domain as well as the amino acid region 69–92 found in p47 (DNRVTSFRDLIHDQDEEEEEEEGQ). The p37 UBX domain is 63% identical to the p47 UBX domain, and the p37 SEP domain is 72% identical to the p47 SEP domain. By deleting amino acids 69–92 from p47, we were able to make a p47 variant (Δ69–92 p47) that behaves like p37 in the p97 ATPase assay (Fig. 2*A*) and the Golgi reassembly assay (Fig. 6 and *SI Appendix*, Fig. S5). After analysis of two additional p47 variants, Δ83–90 p47 and 83–88 (DE₅ to NQ₅) p47, we concluded that the distance generated by 69–92 is the primary determinant of p37-like behavior, as opposed to the acidic charge of the linker. More importantly, Δ69–92 p47 failed to activate disease mutants, which therefore suggests that the same general mechanism used by p37 to activate p97 is also used by p47 to cause the phase 2 rebound of WT p97 (Fig. 6 and *SI Appendix*, Fig. S8).

Potential Model for the Role of p97 Disease Mutants in Defective Cofactor-Regulated ATPase Activity. To summarize the results we have obtained: (*i*) p97 disease mutants lack a biphasic effect in the presence of WT p47; (*ii*) p97 disease mutants cannot be activated by p37 or by a p47 variant (Δ69–92 p47) that mimics p37; (*iii*) p97 disease mutants can be inhibited by WT p47; and (*iv*) p97 disease mutants and WT p97 can interact with p37, p47, or p47 variants in a similar manner, based on pull-down and SPR experiments. We suggest a possible model by which p97 cofactors activate the D2-domain ATPase during the ATPase cycle. Binding at the N domain triggers a conformational change to convert D1 to the ADP-open state, which allows more ATP to bind to D1, thereby stimulating the D2 ATPase. This is the established mechanism by which p97 disease mutants activate D2 activity (20), and explains why no additional activation can be observed in these mutants (Fig. 6 and *SI Appendix*, Fig. S8).

In conclusion, our results suggest a general model for cofactor-regulated p97 ATPase activity involving cofactors that bind to the N domain of WT p97. In the model, the cofactors induce conformation changes that regulate ADP/ATP binding to the D1 domain, which in turn controls the D1 and D2 ATPase cycles. The model is consistent with a recently proposed model explaining abnormal ATPase activity in p97 disease mutants. An altered N-domain conformation leads to abnormal ADP/ATP binding to the D1 domain and causes higher basal D2 ATPase activity in these disease mutants (23). As further support of our findings, several other AAA ATPase proteins are also regulated by cofactors. For example, cytoplasmic dynein is activated by dynactin–cargo adapter complexes (63). The ER-localized AAA ATPase Torsin is activated by lamin-associated polypeptide 1 (LAP1). Vps4 ATPase regulates the endosomal sorting complex required for transport (ESCRT) and is activated by ESCRT-III and the cofactor Vta1 (64). Finally, the activity of *N*-ethyl-maleimide–sensitive factor (NSF) is stimulated by SNAP–SNARE complexes (65–67).

Although the regulation of p97 activity has been extensively studied in terms of its intrinsic ATPase activity, more research remains to be done. Investigation into the differences between p97's interaction with p37 and p47, in addition to other p97 cofactors, will provide a more complete understanding of cofactor-regulated p97 activity. Furthermore, examination of the effects of not only cofactors but also substrates on p97 regulation is a potential future step. We believe that the results of our study will be critical to unlocking the molecular mechanisms of the function of WT and disease mutant p97 ATPases and will assist ongoing efforts to develop therapeutic agents targeting p97 disease mutants.

Materials and Methods

Materials and detailed methods are described in *SI Appendix, Methods*.

ATPase Assay. Purified p97 (25 μL of 50 μM) was diluted in 30 mL of assay buffer [10 mL of 5× assay buffer A (1× = 50 mM Tris pH 7.4, 20 mM MgCl2, 1 mM EDTA), 20 mL water, 50 μL 0.5M TCEP, and 50 μL 10% Triton]. Thirty microliters of this solution and 10 μL of p97 cofactor (0–4,000 nM) were dispensed into each well of a 96-well plate, followed by 10 μL of 1,000 μM or 4,000 μM ATP (pH 7.5). After 35 min at room temperature, the reactions were stopped by adding 50 μL of BIOMOL Green reagent (Enzo Life Sciences). Absorbance at 635 nm was measured after 4 min. Eight final ATP concentrations were used to determine steady-state kinetic constants as previously described (22). Michaelis Menten constants were calculated from 8 replicates using GraphPad Prism 6.0.

Surface Plasmon Resonance. Binding affinities for p37 and p47 cofactors to p97 proteins were measured on a Biacore 4000 instrument. Neutravidin-coated sensor chips were prepared as described previously (22), and p97 proteins were immobilized in 10 mM HEPES, pH 7.5, 150 mM NaCl, 0.5 mM TCEP, 0.05% Tween 20 to 500–600 RU by injecting 4–6 μg/mL protein for 2 min. Binding of cofactor proteins was measured in 25 mM Tris, pH 7.5, 150 mM NaCl, 10 mM MgCl₂, 0.5 mM TCEP, 0.05% Tween 20, and 0.1% Prionex (Calbiochem) at 20 °C. Sensorgrams were reduced, double referenced, and fit to a 1:1 kinetic interaction model (p37) or to an equilibrium binding model for a 1:1 interaction (F253S p47) or a 2:1 interaction [WT p47, Δ69-92 p47, Δ83-92 p47, and 83-88 (DE5to NQ5) p47] in Scrubber 2 (BioLogic Software).

p97-Mediated Postmitotic Golgi Reassembly Assay. The assay was carried out in vitro as described previously (36, 47). Purified rat liver Golgi stacks were treated with mitotic cytosol, and the resulting membrane fragments were incubated with purified p97/p47, p97/Δ69-92 p47, or p97/p37 proteins for reassembly. Membranes were processed for EM, and the results were quantified to estimate the activity of membrane fusion to form cisternal membranes. Mitotic Golgi fragments were normalized to 0%. Reassembly with WT p97 (167 nM hexamer) and p47 (167 nM trimer) was normalized to 100%. The results represent the mean of at least ten EM images ± SEM.

1. Ye Y, Shibata Y, Yun C, Ron D, Rapoport TA (2004) A membrane protein complex mediates retro-translocation from the ER lumen into the cytosol. *Nature* 429(6994):841–847.

2. Ju JS, et al. (2009) Valosin-containing protein (VCP) is required for autophagy and is disrupted in VCP disease. *J Cell Biol* 187(6):875–888.

3. Tresse E, et al. (2010) VCP/p97 is essential for maturation of ubiquitin-containing autophagosomes and this function is impaired by mutations that cause IBMPFD. *Autophagy* 6(2):217–227.

4. Ramadan K, et al. (2007) Cdc48/p97 promotes reformation of the nucleus by extracting the kinase Aurora B from chromatin. *Nature* 450(7173):1258–1262.

5. Meyer HH, Wang Y, Warren G (2002) Direct binding of ubiquitin conjugates by the mammalian p97 adaptor complexes, p47 and Ufd1-Npl4. *EMBO J* 21(21):5645–5652.

6. Kakizuka A (2008) Roles of VCP in human neurodegenerative disorders. *Biochem Soc Trans* 36(Pt 1):105–108.

7. Watts GD, et al. (2004) Inclusion body myopathy associated with Paget disease of bone and frontotemporal dementia is caused by mutant valosin-containing protein. *Nat Genet* 36(4):377–381.

8. Le Ber I, et al.; French Research Network on FTLD/FTLD-ALS (2014) hnRNPA2B1 and hnRNPA1 mutations are rare in patients with "multisystem proteinopathy" and frontotemporal lobar degeneration phenotypes. *Neurobiol Aging* 35(4):e5–e6.

9. Johnson JO, et al.; ITALSGEN Consortium (2010) Exome sequencing reveals VCP mutations as a cause of familial ALS. *Neuron* 68(5):857–864.

10. DeJesus-Hernandez M, et al. (2011) Novel p.Ile151Val mutation in VCP in a patient of African American descent with sporadic ALS. *Neurology* 77(11):1102–1103.

11. Koppers M, et al. (2012) VCP mutations in familial and sporadic amyotrophic lateral sclerosis. *Neurobiol Aging* 33(4):e7–e13.

12. Hirano M, et al. (October 16, 2014) VCP gene analyses in Japanese patients with sporadic amyotrophic lateral sclerosis identify a new mutation. *Neurobiol Aging*, 10.1016/j.neurobiolaging.2014.10.012.

13. Majounie E, et al. (2012) Mutational analysis of the VCP gene in Parkinson's disease. *Neurobiol Aging* 33(1):e1–e2.

14. Kim HJ, et al. (2013) Mutations in prion-like domains in hnRNPA2B1 and hnRNPA1 cause multisystem proteinopathy and ALS. *Nature* 495(7442):467–473.

15. Ching JK, et al. (2013) mTOR dysfunction contributes to vacuolar pathology and weakness in valosin-containing protein associated inclusion body myopathy. *Hum Mol Genet* 22(6):1167–1179.

16. Weihl CC, Miller SE, Hanson PI, Pestronk A (2007) Transgenic expression of inclusion body myopathy associated mutant p97/VCP causes weakness and ubiquitinated protein inclusions in mice. *Hum Mol Genet* 16(8):919–928.

17. Huyton T, et al. (2003) The crystal structure of murine p97/VCP at 3.6 Å. *J Struct Biol* 144(3):337–348.

18. DeLaBarre B, Brunger AT (2003) Complete structure of p97/valosin-containing protein reveals communication between nucleotide domains. *Nat Struct Biol* 10(10):856–863.

19. Halawani D, et al. (2009) Hereditary inclusion body myopathy-linked p97/VCP mutations in the NH2 domain and the D1 ring modulate p97/VCP ATPase activity and D2 ring conformation. *Mol Cell Biol* 29(16):4484–4494.

20. Niwa H, et al. (2012) The role of the N-domain in the ATPase activity of the mammalian AAA ATPase p97/VCP. *J Biol Chem* 287(11):8561–8570.

21. Manno A, Noguchi M, Fukushi J, Motohashi Y, Kakizuka A (2010) Enhanced ATPase activities as a primary defect of mutant valosin-containing proteins that cause inclusion body myopathy associated with Paget disease of bone and frontotemporal dementia. *Genes Cells* 15(8):911–922.

22. Chou TF, et al. (2014) Specific inhibition of p97/VCP ATPase and kinetic analysis demonstrate interaction between D1 and D2 ATPase domains. *J Mol Biol* 426(15):2886–2899.

23. Tang WK, Xia D (2013) Altered intersubunit communication is the molecular basis for functional defects of pathogenic p97 mutants. *J Biol Chem* 288(51):36624–36635.

24. Tang WK, et al. (2010) A novel ATP-dependent conformation in p97 N-D1 fragment revealed by crystal structures of disease-related mutants. *EMBO J* 29(13):2217–2229.

25. Dreveny I, et al. (2004) Structural basis of the interaction between the AAA ATPase p97/VCP and its adaptor protein p47. *EMBO J* 23(5):1030–1039.

26. Uchiyama K, et al. (2002) VCIP135, a novel essential factor for p97/p47-mediated membrane fusion, is required for Golgi and ER assembly in vivo. *J Cell Biol* 159(5):855–866.

27. Meyer HH, Shorter JG, Seemann J, Pappin D, Warren G (2000) A complex of mammalian Ufd1 and Npl4 links the AAA-ATPase, p97, to ubiquitin and nuclear transport pathways. *EMBO J* 19(10):2181–2192.

28. Schuberth C, Buchberger A (2008) UBX domain proteins: Major regulators of the AAA ATPase Cdc48/p97. *Cell Mol Life Sci* 65(15):2360–2371.

29. Kondo H, et al. (1997) p47 is a cofactor for p97-mediated membrane fusion. *Nature* 388(6637):75–78.

30. Meyer HH, Kondo H, Warren G (1998) The p47 co-factor regulates the ATPase activity of the membrane fusion protein, p97. *FEBS Lett* 437(3):255–257.

31. Fernández-Sáiz V, Buchberger A (2010) Imbalances in p97 co-factor interactions in human proteinopathy. *EMBO Rep* 11(6):479–485.

32. Erzurumlu Y, et al. (2013) A unique IBMPFD-related P97/VCP mutation with differential binding pattern and subcellular localization. *Int J Biochem Cell Biol* 45(4):773–782.

33. Ritz D, et al. (2011) Endolysosomal sorting of ubiquitylated caveolin-1 is regulated by VCP and UBXD1 and impaired by VCP disease mutations. *Nat Cell Biol* 13(9):1116–1123.

34. Uchiyama K, et al. (2006) p37 is a p97 adaptor required for Golgi and ER biogenesis in interphase and at the end of mitosis. *Dev Cell* 11(6):803–816.

35. Rabouille C, et al. (1998) Syntaxin 5 is a common component of the NSF- and p97-mediated reassembly pathways of Golgi cisternae from mitotic Golgi fragments in vitro. *Cell* 92(5):603–610.

36. Wang Y, Satoh A, Warren G, Meyer HH (2004) VCIP135 acts as a deubiquitinating enzyme during p97-p47-mediated reassembly of mitotic Golgi fragments. *J Cell Biol* 164(7):973–978.

37. Yuan X, et al. (2004) Structure, dynamics and interactions of p47, a major adaptor of the AAA ATPase, p97. *EMBO J* 23(7):1463–1473.

38. Walker JE, Saraste M, Runswick MJ, Gay NJ (1982) Distantly related sequences in the alpha- and beta-subunits of ATP synthase, myosin, kinases and other ATP-requiring enzymes and a common nucleotide binding fold. *EMBO J* 1(8):945–951.

39. Rouiller I, Butel VM, Latterich M, Milligan RA, Wilson-Kubalek EM (2000) A major conformational change in p97 AAA ATPase upon ATP binding. *Mol Cell* 6(6):1485–1490.

40. Soukenik M, et al. (2004) The SEP domain of p47 acts as a reversible competitive inhibitor of cathepsin L. *FEBS Lett* 576(3):358–362.

41. Yuan X, et al. (2001) Solution structure and interaction surface of the C-terminal domain from p47: A major p97-cofactor involved in SNARE disassembly. *J Mol Biol* 311(2):255–263.

42. Kaneko Y, Tamura K, Totsukawa G, Kondo H (2010) Isolation of a point-mutated p47 lacking binding affinity to p97ATPase. *FEBS Lett* 584(18):3873–3877.

43. Beuron F, et al. (2006) Conformational changes in the AAA ATPase p97-p47 adaptor complex. *EMBO J* 25(9):1967–1976.

44. Hänzelmann P, Buchberger A, Schindelin H (2011) Hierarchical binding of cofactors to the AAA ATPase p97. *Structure* 19(6):833–843.

45. Chia WS, Chia DX, Rao F, Bar Nun S, Geifman Shochat S (2012) ATP binding to p97/VCP D1 domain regulates selective recruitment of adaptors to its proximal N-domain. *PLoS ONE* 7(12):e50490.

46. Beuron F, et al. (2003) Motions and negative cooperativity between p97 domains revealed by cryo-electron microscopy and quantised elastic deformational model. *J Mol Biol* 327(3):619–629.

47. Tang D, Xiang Y, Wang Y (2010) Reconstitution of the cell cycle-regulated Golgi disassembly and reassembly in a cell-free system. *Nat Protoc* 5(4):758–772.

48. Krick R, et al. (2010) Cdc48/p97 and Shp1/p47 regulate autophagosome biogenesis in concert with ubiquitin-like Atg8. *J Cell Biol* 190(6):965–973.

49. Chou T-F, et al. (2011) Reversible inhibitor of p97, DBeQ, impairs both ubiquitin-dependent and autophagic protein clearance pathways. *Proc Natl Acad Sci USA* 108(12):4834–4839.

50. Chou TF, Li K, Frankowski KJ, Schoenen FJ, Deshaies RJ (2013) Structure-activity relationship study reveals ML240 and ML241 as potent and selective inhibitors of p97 ATPase. *ChemMedChem* 8(2):297–312.

51. Polucci P, et al. (2013) Alkylsulfanyl-1,2,4-triazoles, a new class of allosteric valosine containing protein inhibitors. Synthesis and structure-activity relationships. *J Med Chem* 56(2):437–450.

52. Magnaghi P, et al. (2013) Covalent and allosteric inhibitors of the ATPase VCP/p97 induce cancer cell death. *Nat Chem Biol* 9(9):548–556.

53. Siderovski DP, Willard FS (2005) The GAPs, GEFs, and GDIs of heterotrimeric G-protein alpha subunits. *Int J Biol Sci* 1(2):51–66.

54. Li J, Richter K, Reinstein J, Buchner J (2013) Integration of the accelerator Aha1 in the Hsp90 co-chaperone cycle. *Nat Struct Mol Biol* 20(3):326–331.

55. Singh M, Shah V, Tatu U (2014) A novel C-terminal homologue of Aha1 co-chaperone binds to heat shock protein 90 and stimulates its ATPase activity in *Entamoeba histolytica*. *J Mol Biol* 426(8):1786–1798.

56. Li J, Buchner J (2013) Structure, function and regulation of the Hsp90 machinery. *Biom J* 36(3):106–117.

57. Li G, Huang C, Zhao G, Lennarz WJ (2012) Interprotomer motion-transmission mechanism for the hexameric AAA ATPase p97. *Proc Natl Acad Sci USA* 109(10):3737–3741.

58. Huang C, Li G, Lennarz WJ (2012) Dynamic flexibility of the ATPase p97 is important for its interprotomer motion transmission. *Proc Natl Acad Sci USA* 109(25):9792–9797.

59. Richly H, et al. (2005) A series of ubiquitin binding factors connects CDC48/p97 to substrate multiubiquitylation and proteasomal targeting. *Cell* 120(1):73–84.

60. Briggs LC, et al. (2008) Analysis of nucleotide binding to P97 reveals the properties of a tandem AAA hexameric ATPase. *J Biol Chem* 283(20):13745–13752.

61. Nishikori S, Esaki M, Yamanaka K, Sugimoto S, Ogura T (2011) Positive cooperativity of the p97 AAA ATPase is critical for essential functions. *J Biol Chem* 286(18):15815–15820.

62. Alexandru G, et al. (2008) UBXD7 binds multiple ubiquitin ligases and implicates p97 in HIF1alpha turnover. *Cell* 134(5):804–816.

63. McKenney RJ, Huynh W, Tanenbaum ME, Bhabha G, Vale RD (2014) Activation of cytoplasmic dynein motility by dynactin-cargo adapter complexes. *Science* 345(6194):337–341.

64. Davies BA, et al. (2014) Vps4 stimulatory element of the cofactor Vta1 contacts the ATPase Vps4 α7 and α9 to stimulate ATP hydrolysis. *J Biol Chem* 289(41):28707–28718.

65. Morgan A, Dimaline R, Burgoyne RD (1994) The ATPase activity of *N*-ethylmaleimide-sensitive fusion protein (NSF) is regulated by soluble NSF attachment proteins. *J Biol Chem* 269(47):29347–29350.

66. Zhao C, Matveeva EA, Ren Q, Whiteheart SW (2010) Dissecting the *N*-ethylmaleimide-sensitive factor: Required elements of the N and D1 domains. *J Biol Chem* 285(1):761–772.

67. Vivona S, et al. (2013) Disassembly of all SNARE complexes by *N*-ethylmaleimide-sensitive factor (NSF) is initiated by a conserved 1:1 interaction between α-soluble NSF attachment protein (SNAP) and SNARE complex. *J Biol Chem* 288(34):24984–24991.